J Sci Comput (2011) 47: 239–257
DOI 10.1007/s10915-010-9434-6

Local-Structure-Preserving Discontinuous Galerkin Methods with Lax-Wendroff Type Time Discretizations for Hamilton-Jacobi Equations

Wei Guo · Fengyan Li · Jianxian Qiu

Received: 16 June 2010 / Revised: 28 October 2010 / Accepted: 2 November 2010 /
Published online: 10 November 2010

Abstract In this paper, a family of high order numerical methods are designed to solve the Hamilton-Jacobi equation for the viscosity solution. In particular, the methods start with a hyperbolic conservation law system closely related to the Hamilton-Jacobi equation. The compact one-step one-stage Lax-Wendroff type time discretization is then applied together with the local-structure-preserving discontinuous Galerkin spatial discretization. The resulting methods have lower computational complexity and memory usage on both structured and unstructured meshes compared with some standard numerical methods, while they are capable of capturing the viscosity solutions of Hamilton-Jacobi equations accurately and reliably. A collection of numerical experiments is presented to illustrate the performance of the methods.

Keywords Local-structure-preserving · Discontinuous Galerkin method · Lax-Wendroff type time discretization · Limiter · WENO scheme · High order accuracy · Hamilton-Jacobi equation

F. Li was supported in part by the NSF grant DMS-0652481, NSF CAREER award DMS-0847241 and an Alfred P. Sloan Research Fellowship.
J. Qiu was supported in part by NSFC grants 10931004, 1081112028 and 10871093.

W. Guo · J. Qiu (✉)
Department of Mathematics, Nanjing University, Nanjing, Jiangsu 210093, P.R. China
e-mail: jxqiu@nju.edu.cn

W. Guo
e-mail: wguo126@gmail.com

F. Li
Department of Mathematical Sciences, Rensselaer Polytechnic Institute, Troy, NY 12180, USA
e-mail: lif@rpi.edu

J. Qiu
School of Mathematical Sciences, Xiamen University, Xiamen, Fujian 361005, P.R. China

1 Introduction

We consider the Hamilton-Jacobi (HJ) equation

$$\begin{cases} \phi_t + H(\nabla\phi) = 0, & \text{in } \Omega \times [0,T], \\ \phi(\mathbf{x},0) = \phi_0(\mathbf{x}), & \text{in } \Omega, \end{cases} \tag{1.1}$$

with suitable boundary conditions and $H(\cdot)$ is the Hamiltonian. Such equations arise in various applications, such as optimal control, differential games, image processing and computer vision. Viscosity solutions were introduced and studied [11, 12] to single out physically relevant solutions of (1.1), and these solutions are Lipschitz continuous but may have discontinuous derivatives even for smooth initial and boundary conditions. The goal of this paper is to develop a family of high order numerical methods to solve the HJ equation for the viscosity solution accurately and reliably. In particular, we start with rewriting the HJ equation (1.1) into a conservation law system for $\mathbf{w} = \nabla\phi$,

$$\begin{cases} \mathbf{w}_t + \nabla H(\mathbf{w}) = 0, & \text{in } \Omega \times [0,T], \\ \mathbf{w}(x,y,0) = \nabla\phi_0(x,y), & \text{in } \Omega, \end{cases} \tag{1.2}$$

then the compact one-step one-stage Lax-Wendroff type time discretization is applied together with the local-structure-preserving discontinuous Galerkin spatial discretization. The missing constant in ϕ is further recovered according to the original equation (1.1).

The Lax-Wendroff type time discretization, used here as an alternative to the widely used one-step multi-stage Runge-Kutta methods when solving (1.1) or hyperbolic conservation laws, is a one-step one-stage and therefore compact and low-storage time discretization procedure. Also called Taylor type or Cauchy-Kowalewski type time discretization in the literature, this procedure is based on the classical Lax-Wendroff scheme [20], and it relies on converting all (or partial, when approximations with certain accuracy are expected) time derivatives in a temporal Taylor expansion of the solution into spatial derivatives by repeatedly using the underlying differential equation and its differentiated forms.

As a class of finite element methods with the distinct feature of using discontinuous piecewise functions as approximations, discontinuous Galerkin (DG) methods are chosen in this paper as the spatial discretization due to their many attractive properties, such as the ease in handling complicated geometries and boundary conditions, the flexibility in using various local approximating functions (polynomials, divergence-free functions, plane-wave functions) [5, 15, 36] or approximations with different local accuracy, the local conservation property when solving the conservation laws, and the compactness to achieve high order accuracy and hence efficient parallel implementation. These properties also contribute to the growing popularity of DG methods in many applications, e.g. [1, 7, 8, 32, 35].

When DG methods are applied to HJ equations, the difficulty comes from that such equations generally are not in the divergence form. This prevents one from using the standard procedure to design DG methods for these equations. Our proposed methods are closely related to the pioneering work by Hu and Shu [16] which was later reinterpreted and simplified in [23]. This work is based on the connection between the HJ equation and the conservation law system, that is, the gradient $\mathbf{w} = \nabla\phi$ of the solution ϕ to the HJ equation satisfies (1.2), a weakly hyperbolic conservation law system. The new feature of the system (1.2) is the inter-dependence of the components of $\mathbf{w}$ when (1.1) is multi-dimensional in space, due to the fact $\nabla \times \mathbf{w} = \nabla \times \nabla\phi = 0$. In [23], locally curl-free polynomials are used to approximate $\mathbf{w} = \nabla\phi$ in the standard DG framework for the hyperbolic system, the missing constant

in ϕ is then recovered according to the original equation (1.1). Such DG methods are one example of the local-structure-preserving DG methods [5, 15, 23, 24, 36], designed for certain applications in order to result better cost efficiency. And this efficiency is achieved by incorporating the a priori knowledge of the exact solutions into the choice of local approximating functions in the DG formulations, largely due to the flexibility of DG methods in using various local approximations especially when compared with the classical finite element methods. Other DG methods to *directly* solve HJ equations (1.1) for ϕ include the one in [3], a method with the lowest computational complexity among all available DG methods for HJ equations in multi-dimensional cases, with its performance for nonconvex Hamiltonians $H(\cdot)$ yet to be investigated. Another one is the central DG method recently developed in [22]. This work suggests a general procedure to design DG methods for problems in the non-divergence form, and the method relies on two sets of meshes and hence has certain complexity when being implemented on non-rectangular meshes. Besides DG methods, other high order numerical methods for HJ equations include finite difference schemes [18, 26–28, 31] which are simple to implement yet generally require structured meshes, and the methods as in [21, 37] which use nodal based approximations on unstructured meshes yet involve complicated reconstruction procedure to achieve high order accuracy.

In order for the proposed methods to converge to the viscosity solutions, nonlinear limiters are necessary as in [2, 16, 22] especially for some examples with the nonconvex Hamiltonian. In this paper, we adopt the WENO limiter strategies developed in [30, 38]. Such limiting procedures, based on the WENO reconstruction used in high order finite volume methods [17, 19, 25, 37], are very robust, and they can simultaneously achieve the uniform high order accuracy in numerical solutions and the reliable transition around non-smooth features such as shocks or around sharp gradient structures.

Compared with using the standard piecewise polynomial functions in DG methods, advantages in using the locally curl-free approximations to solve HJ equations include the reduction of the computational cost and memory usage, as well as a more natural framework for analysis. One can refer to [23] for more discussions. Though it is generally more involved to formulate and to code DG methods with the Lax-Wendroff type time discretization (LWDG) [13, 14, 29] compared with DG methods using the Runge-Kutta time-discretization (RKDG) [4, 6–9], the LWDG method is more compact and requires lower storage. It is demonstrated in [29] that the LWDG method is more cost effective and produces sharper discontinuity transition than the RKDG method for certain problems including two-dimensional Euler systems of compressible gas dynamics. Moreover, nonlinear limiters, if used, only need to be applied once during each time step in LWDG methods yet they need to be applied for each inner stage during one Runge-Kutta time step in RKDG methods. This leads to additional cost reduction in computation. The overall cost efficiency of the proposed methods is illustrated through the two dimensional Riemann problem in Sect. 3.2.

The rest of this paper is organized as follows. In Sect. 2, we formulate the local-structure-preserving DG methods with the Lax-Wendroff type time discretization for HJ equations, and some implementation details are also discussed. In Sect. 3, a collection of numerical examples is presented to demonstrate the performance of the proposed methods. The concluding remarks are given in Sect. 4.

2 Description of the Numerical Method

In this section, we present the formulation and some implementation details of a family of local-structure-preserving discontinuous Galerkin methods with the Lax-Wendroff type time

discretization for the two dimensional Hamilton-Jacobi (HJ) equation (1.1). The methods can be similarly formulated for higher dimensional cases.

2.1 Lax-Wendroff Type Time Discretization

Similar as in [16], we first rewrite the HJ equation (1.1) into a weakly hyperbolic conservation law system (1.2) for $\mathbf{w} = (w_1, w_2) = \nabla\phi$. Based on the idea of the classical Lax-Wendroff scheme [20], the Lax-Wendroff type time discretization for (1.2) starts with a temporal Taylor expansion of w_i, $i = 1, 2$,

$$w_i(x, y, t + \Delta t) = w_i(x, y, t) + \Delta t (w_i)_t + \frac{\Delta t^2}{2}(w_i)_{tt} + \frac{\Delta t^3}{6}(w_i)_{ttt} + \cdots, \tag{2.1}$$

here Δt is the time step. The time derivatives in (2.1) are then converted into spatial derivatives by repeatedly using the equation system (1.2) and its differentiated versions. In order to achieve kth order accuracy in time, one only needs to work with the first k time derivatives in (2.1), namely, $\frac{\partial w_i}{\partial t}, \ldots, \frac{\partial^k w_i}{\partial t^k}$, $i = 1, 2$. In this paper, we will proceed up to third order accuracy in time, although the procedure described here can be naturally extended to higher order accuracy.

By using the governing equation system (1.2) and its differentiated forms, and with the notations $H_i(w_1, w_2) = \frac{\partial H(w_1, w_2)}{\partial w_i}$, $H_{ij}(w_1, w_2) = \frac{\partial^2 H(w_1, w_2)}{\partial w_i \partial w_j}$, $i, j = 1, 2$, one gets

$$\begin{aligned}
(w_1)_t &= -(H(w_1, w_2))_x = -H_1(w_1, w_2)(w_1)_x - H_2(w_1, w_2)(w_2)_x,\\
(w_2)_t &= -(H(w_1, w_2))_y = -H_1(w_1, w_2)(w_1)_y - H_2(w_1, w_2)(w_2)_y,\\
(w_1)_{tt} &= -(H(w_1, w_2))_{tx} = -(H_1(w_1, w_2)(w_1)_t + H_2(w_1, w_2)(w_2)_t)_x\\
&= -(H_{11}(w_1, w_2)(w_1)_x + H_{12}(w_1, w_2)(w_2)_x)(w_1)_t - H_1(w_1, w_2)(w_1)_{xt}\\
&\quad - (H_{12}(w_1, w_2)(w_1)_x + H_{22}(w_1, w_2)(w_2)_x)(w_2)_t - H_2(w_1, w_2)(w_2)_{xt},\\
(w_2)_{tt} &= -(H(w_1, w_2))_{ty} = -(H_1(w_1, w_2)(w_1)_t + H_2(w_1, w_2)(w_2)_t)_y\\
&= -(H_{11}(w_1, w_2)(w_1)_y + H_{12}(w_1, w_2)(w_2)_y)(w_1)_t - H_1(w_1, w_2)(w_1)_{yt}\\
&\quad - (H_{12}(w_1, w_2)(w_1)_y + H_{22}(w_1, w_2)(w_2)_y)(w_2)_t - H_2(w_1, w_2)(w_2)_{yt},\\
(w_1)_{xt} &= -(H_1(w_1, w_2)(w_1)_x + H_2(w_1, w_2)(w_2)_x)_x\\
&= -(H_{11}(w_1, w_2)(w_1)_x{}^2 + 2H_{12}(w_1, w_2)(w_1)_x(w_2)_x + H_{22}(w_1, w_2)(w_2)_x{}^2)\\
&\quad - H_1(w_1, w_2)(w_1)_{xx} - H_2(w_1, w_2)(w_2)_{xx},\\
(w_1)_{yt} &= -(H_1(w_1, w_2)(w_1)_x + H_2(w_1, w_2)(w_2)_x)_y\\
&= -(H_{11}(w_1, w_2)(w_1)_x(w_1)_y + H_{12}(w_1, w_2)((w_1)_x(w_2)_y + (w_1)_y(w_2)_x)\\
&\quad + H_{22}(w_1, w_2)(w_2)_x(w_2)_y) - H_1(w_1, w_2)(w_1)_{xy} - H_2(w_1, w_2)(w_2)_{xy},\\
(w_2)_{xt} &= -(H(w_1, w_2))_{yx} = (w_1)_{yt},\\
(w_2)_{yt} &= -(H_1(w_1, w_2)(w_1)_y + H_2(w_1, w_2)(w_2)_y)_y\\
&= -(H_{11}(w_1, w_2)(w_1)_y{}^2 + 2H_{12}(w_1, w_2)(w_1)_y(w_2)_y + H_{22}(w_1, w_2)(w_2)_y{}^2)\\
&\quad - H_1(w_1, w_2)(w_1)_{yy} - H_2(w_1, w_2)(w_2)_{yy}.
\end{aligned}$$

$$(w_1)_{ttt} = -(H(w_1, w_2))_{xtt} = -\mathcal{G}_x, \qquad (w_2)_{ttt} = -(H(w_1, w_2))_{ytt} = -\mathcal{G}_y,$$

with

$$\begin{aligned}\mathcal{G} &= (H(w_1, w_2))_{tt} \\ &= H_{11}(w_1, w_2)(w_1)_t{}^2 + 2H_{12}(w_1, w_2)(w_1)_t(w_2)_t + H_{22}(w_1, w_2)(w_2)_t{}^2 \\ &\quad + H_1(w_1, w_2)(w_1)_{tt} + H_2(w_1, w_2)(w_2)_{tt}.\end{aligned}$$

Now one can replace the time derivatives of w_i with its spatial derivatives according to the formulas derived above, and approximate (2.1) and therefore (1.2) with

$$\begin{cases} w_1(x, y, t + \Delta t) = w_1(x, y, t) - \Delta t \mathcal{H}_x, \\ w_2(x, y, t + \Delta t) = w_2(x, y, t) - \Delta t \mathcal{H}_y. \end{cases} \tag{2.2}$$

In particular, (2.2) provides a second order approximation when

$$\mathcal{H} = H + \frac{\Delta t}{2}(H_1(w_1, w_2)(w_1)_t + H_2(w_1, w_2)(w_2)_t) \tag{2.3}$$

and a third order approximation when

$$\mathcal{H} = H + \frac{\Delta t}{2}(H_1(w_1, w_2)(w_1)_t + H_2(w_1, w_2)(w_2)_t) + \frac{\Delta t^2}{6}\mathcal{G}. \tag{2.4}$$

Next, local-structure-preserving discontinuous Galerkin methods will be formulated to discretize $\mathcal{H}_x$ and $\mathcal{H}_y$ in (2.2).

2.2 Local-Structure-Preserving Discontinuous Galerkin Spatial Discretization

Let $\mathcal{T}_h = \{K\}$ denote a regular triangulation of the computational domain Ω, with the element K being a triangle, a rectangle or a more general polygon, and the edge of K as e. And $h = \max_{K\in\mathcal{T}_h} \operatorname{diam}(K)$. Let $\mathbf{V}_h$ denote a finite dimensional discrete space consisting of piecewise smooth functions with respect to $\mathcal{T}_h$, which will be specified later. The discontinuous Galerkin (DG) discretization for (2.2) is defined as follows: find $\mathbf{w}_h^{n+1}(x, y) = (w_{1,h}^{n+1}(x, y), w_{2,h}^{n+1}(x, y)) \in \mathbf{V}_h$, such that $\forall\, \mathbf{v} = (v_1, v_2) \in \mathbf{V}_h$, $\forall\, K \in \mathcal{T}_h$,

$$\begin{aligned}\int_K w_{1,h}^{n+1} v_1 dxdy = \int_K w_{1,h}^n v_1 dxdy + \Delta t_n \Bigg(\int_K \mathcal{H}(w_{1,h}^n, w_{2,h}^n)(v_1)_x dxdy \\ - \sum_{e\subset\partial K} \int_e \hat{\mathcal{H}}_{1,e,K}(w_{1,h}^n, w_{2,h}^n) v_1 ds \Bigg)\end{aligned} \tag{2.5}$$

and

$$\begin{aligned}\int_K w_{2,h}^{n+1} v_2 dxdy = \int_K w_{2,h}^n v_2 dxdy + \Delta t_n \Bigg(\int_K \mathcal{H}(w_{1,h}^n, w_{2,h}^n)(v_2)_y dxdy \\ - \sum_{e\subset\partial K} \int_e \hat{\mathcal{H}}_{2,e,K}(w_{1,h}^n, w_{2,h}^n) v_2 ds \Bigg)\end{aligned} \tag{2.6}$$

for $n = 0, 1, 2, \ldots$. In (2.5)–(2.6), $\mathbf{w}_h^n$ approximates the solution of (2.1) (and therefore (1.2)) at t^n, and $\Delta t_n = t^{n+1} - t^n$. The function $\hat{\mathcal{H}}_{i,e,K}$ $(i = 1, 2)$ is a consistent and conservative numerical flux [16], and it is related to the so-called generalized Riemann solvers [34] and depends on the numerical solution $\mathbf{w}_h$ and its spatial derivatives from both sides of the element interface $e \subset K$. In this paper, the following Lax-Friedrichs flux is used for $i = 1, 2$,

$$\hat{\mathcal{H}}_{i,e,K}(w_1, w_2) = \frac{1}{2}\left(\mathcal{H}(w_1^-, w_2^-) + \mathcal{H}(w_1^+, w_2^+)\right) n_i - \frac{\alpha_i}{2}(w_i^+ - w_i^-).$$

Here $n = (n_1, n_2)$ is the unit outward normal of K along its edge $e = K \cap K'$, with $\mathbf{w}^- = \mathbf{w}|_K$ and $\mathbf{w}^+ = \mathbf{w}|_{K'}$. And $\alpha_i = \max_{w_1,w_2} |H_i(w_1, w_2)|$, with the maximum taken in the computational domain for $i = 1, 2$. In addition, with $\hat{\mathcal{H}}_{e,K} = (\hat{\mathcal{H}}_{1,e,K}, \hat{\mathcal{H}}_{2,e,K})$, the DG discretization (2.5)–(2.6) can be rewritten more compactly: find $\mathbf{w}_h^{n+1} \in \mathbf{V}_h$, such that $\forall \mathbf{v} \in \mathbf{V}_h$, $\forall K \in \mathcal{T}_h$,

$$\int_K \mathbf{w}_h^{n+1} \cdot \mathbf{v} dx dy = \int_K \mathbf{w}_h^n \cdot \mathbf{v} dx dy + \Delta t_n \left(\int_K \mathcal{H}(\mathbf{w}_h^n) \nabla \cdot \mathbf{v} dx dy - \sum_{e \subset \partial K} \int_e \hat{\mathcal{H}}_{e,K}(\mathbf{w}_h^n) \cdot \mathbf{v} ds \right). \tag{2.7}$$

And $\mathbf{w}_h^0 \in \mathbf{V}_h$ can be initialized through the L^2 projection, namely,

$$\int_K \mathbf{w}_h^0 \cdot \mathbf{v} dx dy = \int_K \nabla \phi_0 \cdot \mathbf{v} dx dy, \quad \forall \mathbf{v} \in \mathbf{V}_h, \forall K \in \mathcal{T}_h. \tag{2.8}$$

To finalize the DG method with the Lax-Wendroff type time discretization defined in (2.7), (2.8), and (2.3) (or (2.4)), one would need to specify the discrete space $\mathbf{V}_h$. By following [23], we take

$$\mathbf{V}_h = \mathbf{V}_h^k = \{(v_1, v_2) : \mathbf{v}|_K = \nabla \phi, \ \phi \in P^k(K), \forall K \in \mathcal{T}_h\}. \tag{2.9}$$

Note the function $\mathbf{v} \in \mathbf{V}_h$ satisfies $\nabla \times \mathbf{v} = 0$ on each $K \in \mathcal{T}_h$, a property of the exact solution $\mathbf{w}$ of (1.2) due to the relation $\nabla \times \mathbf{w} = \nabla \times \nabla \phi = 0$. With such a choice, the method described above is termed as the local-structure-preserving DG (LSP-DG) method with the Lax-Wendroff type time discretization. Similar LSP-DG methods were also investigated in [5, 15, 24, 36], with the objective to develop DG methods with better cost efficiency when solving certain differential equations. Such efficiency is achieved by incorporating the a priori knowledge of the exact solutions into the choice of local approximating functions in the DG formulations, largely due to the flexibility of DG methods in using various local approximations especially when compared with the classical finite element methods. Some advantages in using this locally curl-free discrete space $\mathbf{V}_h^k$ as (2.9) compared with using the standard piecewise polynomial space in DG methods include the reduction of the computational cost and memory usage, as well as a more natural framework for analysis. One can refer to [23] for more details.

Though it is generally more involved to formulate and to code DG methods with the Lax-Wendroff type time discretization (LWDG) [13, 14, 29] compared with DG methods using the Runge-Kutta time-discretization (RKDG) [4, 6–9], the LWDG method is more compact and requires lower storage. To implement the LSP-DG method with the Lax-Wendroff type time discretization defined by (2.7)–(2.9) and (2.3) (or (2.4)), when the mesh $\mathcal{T}_h$ consists of rectangular elements, a local orthogonal basis can be adopted for $\mathbf{V}_h^k$ over each element. For

example, for a rectangular element $K \in \mathcal{T}_h$ with the center (x_0, y_0) and the size $\Delta x \times \Delta y$, the basis functions of $\mathbf{V}_h^k|_K$ can be

$$\begin{aligned}
&\text{for } k=1: \quad \varphi_0^K = (1,0), \qquad \varphi_1^K = (0,1),\\
&\text{for } k=2: \quad \text{add } \varphi_2^K = (\xi,0), \qquad \varphi_3^K = (0,\eta), \qquad \varphi_4^K = (\lambda\eta,\xi),\\
&\text{for } k=3: \quad \text{add } \varphi_5^K = \left(\xi^2 - \frac{1}{12}, 0\right), \qquad \varphi_6^K = \left(2\lambda\xi\eta, \xi^2 - \frac{1}{12}\right),\\
&\qquad\qquad \varphi_7^K = \left(0, \eta^2 - \frac{1}{12}\right), \qquad \varphi_8^K = \left(\eta^2 - \frac{1}{12}, \frac{2}{\lambda}\xi\eta\right).
\end{aligned}$$

Here $\xi = \frac{x-x_0}{\Delta x}$, $\eta = \frac{y-y_0}{\Delta y}$, and $\lambda = \frac{\Delta y}{\Delta x}$. Once the local basis functions are chosen, the numerical solution $\mathbf{w}_h^n$ to (2.6) restricted to K can be expressed as

$$\mathbf{w}_h^n(x,y) = \sum_{l=0}^{L_k} \boldsymbol{\omega}_K^{n,(l)} \varphi_l^K(x,y), \quad \text{for } (x,y) \in K, \tag{2.10}$$

where $L_k = \frac{k(k+3)}{2}$ is the dimension of $\mathbf{V}_h^k|_K$. And the degrees of freedom $\boldsymbol{\omega}_K^{n,(l)}$ are the moments defined by

$$\boldsymbol{\omega}_K^{n,(l)} = \frac{1}{a_l} \int_K \mathbf{w}_h^n \cdot \varphi_l^K \, dxdy, \quad l = 0, 1, \ldots, L_k,$$

with the normalization constant $a_l = \int_K |\varphi_l^K(x,y)|^2 dxdy$. Now $\boldsymbol{\omega}_K^{n,(l)}$ for $K \in \mathcal{T}_h$, $l = 0, 1, \ldots, L_k$ can be evolved based on (2.7)–(2.8) as follows,

$$\begin{aligned}
\boldsymbol{\omega}_K^{n+1,(l)} &= \boldsymbol{\omega}_K^{n,(l)} + \frac{\Delta t_n}{a_l}\left(\int_K \mathcal{H}(\mathbf{w}_h^n)\nabla \cdot \varphi_l^K \, dxdy \right.\\
&\qquad \left. - \sum_{e \subset \partial K} \int_e \hat{\mathcal{H}}_{e,K}(\mathbf{w}_h^n) \cdot \varphi_l^K \, ds\right), \quad n = 0, 1, \ldots,\\
\boldsymbol{\omega}_K^{0,(l)} &= \frac{1}{a_l} \int_K \nabla\phi_0 \cdot \varphi_l^K \, dxdy.
\end{aligned}$$

With these $\{\boldsymbol{\omega}_K^{n,(l)}\}_{K,l,n}$, one obtains $\mathbf{w}_h \in \mathbf{V}_h$ which approximates the solution $\mathbf{w}$ of (1.2) and therefore $\nabla\phi$ for the HJ equation (1.1). The strategies to recover the missing constant in ϕ proposed in [16] are based on Runge-Kutta time discretizations. In this paper, we adopt a similar recovering strategy based on the Lax-Wendroff procedure. Denote q_K as the center of an element K (or the barycenter for general elements), we can update $\phi(q_K, t + \Delta t)$ according to the Taylor expansion

$$\phi(q_K, t+\Delta t) = \phi(q_K,t) + \Delta t \phi_t(q_K,t) + \frac{\Delta t^2}{2}\phi_{tt}(q_K,t) + \frac{\Delta t^3}{6}\phi_{ttt}(q_K,t) + \cdots,$$

where time derivatives are obtained from the spatial derivatives by repeatedly using the governing equations (1.1) and (1.2). This gives the approximation to ϕ at q_K

$$\phi(q_K, t^{n+1}) = \phi(q_K, t^n) - \Delta t_n \mathcal{H}(\mathbf{w}_h^n(q_K)), \tag{2.11}$$

with the second and the third order accuracy when $\mathcal{H}$ is defined in (2.3) and (2.4), respectively. In practice, this procedure only needs to be applied to a few elements, e.g., the corner elements, during the time evolution in the simulation. And the missing constant of ϕ at an arbitrary location $q = (x, y)$ can be recovered through integration

$$\phi_h(q, T) = \phi_h(q_K, T) + \int_q^{q_K} w_{1,h}^N dx + w_{2,h}^N dy \tag{2.12}$$

at the final time step $T = t^N$.

When the mesh $\mathcal{T}_h$ also consists of other shapes of elements such as triangles, the following local basis functions are used for $\mathbf{V}_h^k$ over K:

$$\begin{array}{lll} k=1: & \varphi_0 = (1,0), & \varphi_1 = (0,1), \\ k=2: & \text{add } \varphi_2 = (\xi,0), & \varphi_3 = (0,\eta), \quad \varphi_4 = (\eta,\xi), \\ k=3: & \text{add } \varphi_5 = (\xi^2,0), & \varphi_6 = (2\xi\eta,\xi^2), \quad \varphi_7 = (0,\eta^2), \quad \varphi_8 = (\eta^2,2\xi\eta). \end{array}$$

Here $\xi = \frac{x-x_0}{\sqrt{|K|}}$, $\eta = \frac{y-y_0}{\sqrt{|K|}}$, and (x_0, y_0) and $|K|$ are the barycenter (or other suitable reference points) and the area of K respectively. Note such basis functions, though simple, are not orthogonal, and a local mass matrix of the dimension $L_k \times L_k$ needs to be inverted in each element $K \in \mathcal{T}_h$. Fortunately these small matrices only need to be computed once and they can be stored for later use during the time evolution. For $\mathbf{V}_h^k$ with higher k, the orthogonal basis is preferred for better numerical performance.

In order for the proposed methods to reliably capture the viscosity solution, nonlinear limiters are necessary especially when the Hamiltonian H is nonconvex. Such phenomena was also observed in [2, 16, 22]. In this paper, we adopt the WENO limiter strategies developed in [30] for rectangular meshes and in [38] for triangular meshes. Such limiting procedures are based on the WENO reconstruction used in high order finite volume methods [17, 19, 25, 37]. And when they are applied to an element $K \in \mathcal{T}_h$ which is identified as a troubled cell, all moments of the numerical solutions in this element will be abandoned except the cell average. The abandoned moments will be reconstructed based on the cell averages of the solution in neighboring elements using the WENO methodology. Not like some limiters which may degenerate the accuracy especially of high order schemes when mistakenly used in the smooth region of the solution [4, 7, 9, 22], WENO limiters are very robust, and they can simultaneously achieve the uniform high order accuracy in numerical solutions and the reliable transition around non-smooth features such as shocks or around sharp gradient structures. In our numerical experiments, WENO methods are applied to reconstruct the polynomial of $\mathbf{w}_h^n$, in which the degree of reconstructed polynomial in each small stencil is the same as that of $\mathbf{w}_h^n$ to maintain the order of accuracy of the DG schemes. We use the optimal linear weights to get higher order reconstructions for rectangular meshes, that is we use the third and fifth order WENO reconstructions for P^2 and P^3 cases, respectively. For triangular meshes a fixed set of average linear weights is used in each small stencil for the ease of implementation, that is we use the second and third order WENO type reconstructions for P^2 and P^3 cases, respectively. Though the magnitude of error by this implementation will be a little bigger than those by the implementation with optimal linear weights, the orders of accuracy of the underlying DG methods are maintained by both the implementations. Such implementation strategy also saves computational cost as we do not compute the more complex optimal linear weights, and the negative linear weights can be avoided as well. Note that nonlinear limiters, if used, only need to be applied once during each time step in LWDG methods yet they need to be applied for each inner stage during one Runge-Kutta time step in RKDG methods. This leads to additional cost reduction in computation.

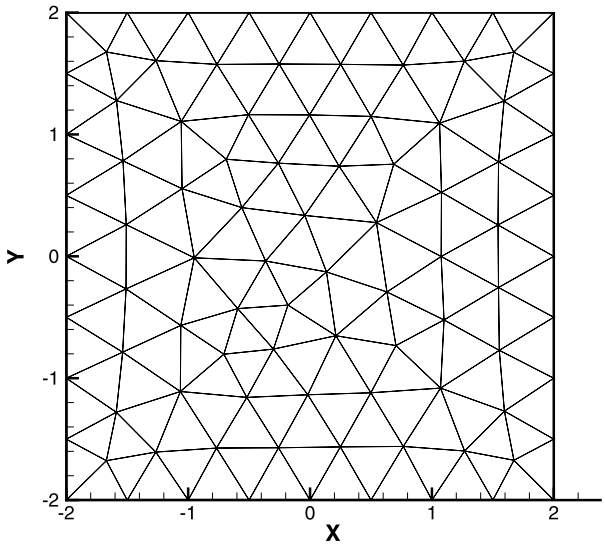

Fig. 1 An unstructured triangular mesh with the characteristic meshsize $h = 1/2$

3 Numerical Results

In this section, a collection of two-dimensional numerical experiments is presented to illustrate the high order accuracy and the reliability of the proposed methods when solving the viscosity solutions of the Hamilton-Jacobi equations. Both uniform rectangular meshes and unstructured triangular meshes are used in the computation. An example of the triangular meshes with the characteristic meshsize $h = 1/2$ is given in Fig. 1. WENO limiters are applied to all examples, though they are not needed for smooth examples and for some nonsmooth examples. In order to decide whether limiters are needed in each mesh element during the simulation, the TVB limiters with the constant $M = 0.01$ [6, 9, 33] are used as the troubled cell indicator. We want to remark that a good choice of the TVB constant M is problem dependent for the reliability and cost efficiency of the limiting procedures. Generally, if M is chosen too large, some cells with spurious oscillation may not be recognized. If M is chosen too small, some good cells will be identified as troubled cells. In this case, the implementation of WENO limiters on these cells will introduce extra computational cost without degenerating the accuracy of the methods.

3.1 Accuracy Tests

In this section, the accuracy of the proposed methods will be examined.

Example 3.1 Consider the Burgers equation

$$\phi_t + \frac{(\phi_x + \phi_y + 1)^2}{2} = 0 \tag{3.1}$$

with the initial condition $\phi_0(x, y) = -\cos(\pi(x + y)/2)$ and the 4-periodic boundary condition. This example involves a convex Hamiltonian. The computation is first carried out on the uniform rectangular meshes. When $t = 0.5/\pi^2$, the solution is still smooth, and the errors and numerical orders of accuracy of the proposed methods are shown in Table 1. The

Table 1 Burgers equation. L_1 and L_∞ errors and numerical orders of accuracy on uniform rectangular meshes with $N_x \times N_y$ cells, $t = 0.5/\pi^2$

	$N_x \times N_y$	With the WENO limiter				Without the limiter			
		L_1 error	order	L_∞ error	order	L_1 error	order	L_∞ error	order
P^2	10×10	2.46E−02		9.12E−02		1.30E−02		5.99E−02	
	20×20	4.73E−03	2.38	2.18E−02	2.07	2.74E−03	2.25	1.44E−02	2.06
	40×40	8.84E−04	2.42	5.26E−03	2.05	6.24E−04	2.14	2.64E−03	2.44
	80×80	1.68E−04	2.40	1.09E−03	2.27	1.50E−04	2.06	5.17E−04	2.35
	160×160	3.82E−05	2.14	1.67E−04	2.71	3.63E−05	2.04	1.20E−04	2.11
P^3	10×10	1.01E−02		3.64E−02		3.13E−03		9.39E−03	
	20×20	3.65E−04	4.79	1.29E−03	4.81	3.62E−04	3.12	1.17E−03	3.01
	40×40	7.24E−05	2.33	2.15E−04	2.59	6.98E−05	2.37	2.11E−04	2.47
	80×80	1.18E−05	2.62	3.47E−05	2.63	1.17E−05	2.57	3.41E−05	2.63
	160×160	1.71E−06	2.79	4.76E−06	2.86	1.70E−06	2.78	4.76E−06	2.84

Table 2 Burgers equation. L_1 and L_∞ errors and numerical orders of accuracy on unstructured triangular meshes with the characteristic meshsize h, $t = 0.5/\pi^2$

	h	With the WENO limiter				Without the limiter			
		L_1 error	order	L_∞ error	order	L_1 error	order	L_∞ error	order
P^2	1/2	3.95E−02		1.72E−01		7.31E−03		4.29E−02	
	1/4	1.04E−02	1.93	4.27E−02	2.01	1.45E−03	2.34	9.69E−03	2.15
	1/8	2.16E−03	2.27	1.13E−02	1.92	2.80E−04	2.37	1.67E−03	2.54
	1/16	4.00E−04	2.43	1.75E−03	2.68	5.71E−05	2.30	3.72E−04	2.16
	1/32	8.20E−05	2.29	3.77E−04	2.22	1.35E−05	2.08	9.05E−05	2.04
P^3	1/2	6.36E−03		3.94E−02		6.31E−04		4.56E−03	
	1/4	3.48E−04	4.19	3.28E−03	3.59	6.54E−05	3.27	7.07E−04	2.69
	1/8	2.40E−05	3.86	1.78E−04	4.20	6.57E−06	3.32	6.65E−05	3.41
	1/16	1.74E−06	3.78	1.92E−05	3.22	8.14E−07	3.01	7.36E−06	3.18
	1/32	1.28E−07	3.76	2.23E−06	3.10	9.53E−08	3.09	7.60E−07	3.28

results confirm the designed accuracy of the schemes, namely, the method is kth order accurate when $\mathbf{V}_h = \mathbf{V}_h^k$ in (2.9) and the first k time derivatives in (2.1) are used. The L_1 and L_∞ errors are computed by using a (6×6)-point Gaussian quadrature formula in each cell. Though the limiter strategy is not needed for this smooth example, we still report the numerical results with the limiter procedure turned on, and these results show that the WENO limiter keeps the designed order of accuracy uniformly.

Next, the computation is done on unstructured triangular meshes. The errors and numerical orders of accuracy of the proposed methods are reported in Table 2. The L_1 and L_∞ errors are computed by a 7-point Gaussian quadrature formula in each cell. Similar accuracy pattern is observed as in the cases with rectangular meshes.

Table 3 The example of $\phi_t - \cos(\phi_x + \phi_y + 1) = 0$. L_1 and L_∞ errors and numerical orders of accuracy on uniform rectangular meshes with $N_x \times N_y$ cells, $t = 0.5/\pi^2$

	$N_x \times N_y$	With the WENO limiter				Without the limiter			
		L_1 error	order	L_∞ error	order	L_1 error	order	L_∞ error	order
P^2	10×10	1.33E−02		6.34E−02		1.05E−02		4.74E−02	
	20×20	2.42E−03	2.46	9.57E−03	2.73	2.17E−03	2.27	9.55E−03	2.31
	40×40	5.57E−04	2.12	2.14E−03	2.16	5.26E−04	2.05	2.14E−03	2.16
	80×80	1.32E−04	2.07	4.66E−04	2.20	1.29E−04	2.02	4.61E−04	2.21
	160×160	3.20E−05	2.05	1.18E−04	1.98	3.19E−05	2.02	1.16E−04	1.99
P^3	10×10	1.73E−02		4.79E−02		1.47E−02		2.25E−02	
	20×20	9.54E−04	4.18	2.26E−03	4.41	1.49E−03	3.31	3.12E−03	2.85
	40×40	2.09E−04	2.19	4.21E−04	2.42	2.24E−04	2.73	4.43E−04	2.81
	80×80	2.75E−05	2.93	5.65E−05	2.90	2.82E−05	2.99	5.73E−05	2.95
	160×160	4.30E−06	2.68	8.42E−06	2.75	4.34E−06	2.70	8.49E−06	2.76

Table 4 The example of $\phi_t - \cos(\phi_x + \phi_y + 1) = 0$. L_1 and L_∞ errors and numerical orders of accuracy on unstructured triangular meshes with the characteristic meshsize h, $t = 0.5/\pi^2$

	h	With the WENO limiter				Without the limiter			
		L_1 error	order	L_∞ error	order	L_1 error	order	L_∞ error	order
P^2	1/2	3.04E−02		1.03E−01		8.45E−03		3.15E−02	
	1/4	6.81E−03	2.16	2.44E−02	2.08	1.45E−03	2.54	7.38E−03	2.09
	1/8	1.46E−03	2.22	5.30E−03	2.20	2.50E−04	2.54	1.49E−03	2.31
	1/16	3.06E−04	2.25	1.44E−03	1.88	4.44E−05	2.50	3.67E−04	2.02
	1/32	7.03E−05	2.12	2.84E−04	2.34	1.20E−05	1.89	8.16E−05	2.17
P^3	1/2	6.29E−03		3.97E−02		8.54E−04		8.18E−03	
	1/4	3.08E−04	4.35	4.21E−03	3.24	1.01E−04	3.08	1.56E−03	2.39
	1/8	2.04E−05	3.92	2.36E−04	4.16	1.41E−05	2.84	1.60E−04	3.29
	1/16	2.00E−06	3.35	1.31E−05	4.17	2.05E−06	2.78	1.27E−05	3.65
	1/32	2.31E−07	3.11	2.35E−06	2.48	2.55E−07	3.01	1.54E−06	3.05

Example 3.2 Consider

$$\phi_t - \cos(\phi_x + \phi_y + 1) = 0 \tag{3.2}$$

with the initial condition $\phi_0(x, y) = -\cos(\pi(x + y)/2)$ and the 4-periodic boundary condition. This example involves a nonconvex Hamiltonian. The computation is first carried out on the uniform rectangular meshes. When $t = 0.5/\pi^2$, the solution is still smooth, and the errors and numerical orders of accuracy of the proposed methods are shown in Table 3. The L_1 and L_∞ errors are computed by using a (6×6)-point Gaussian quadrature formula in each cell. The results confirm the designed accuracy of the proposed methods. Next, we use unstructured triangular meshes. The errors and numerical orders of accuracy are shown in Table 4. A 7-point Gaussian quadrature formula is used to compute the L_1 and L_∞ errors. The expected orders of accuracy are obtained. WENO limiter procedures again are turned

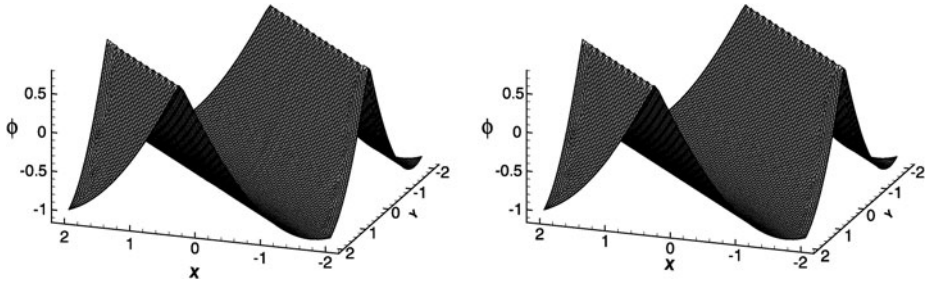

Fig. 2 Burgers equation. The numerical solution at $t = 1.5/\pi^2$ on the unstructured triangular mesh with $h = 1/16$. P^2 (*left*) and P^3 (*right*)

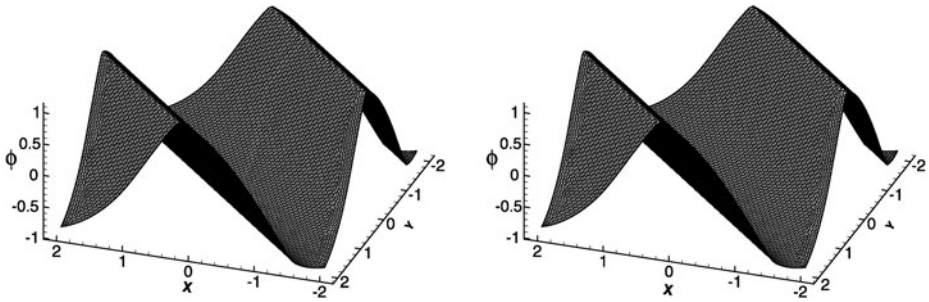

Fig. 3 The example of $\phi_t - \cos(\phi_x + \phi_y + 1) = 0$. The numerical solution at $t = 1.5/\pi^2$ on the unstructured triangular mesh with $h = 1/16$. P^2 (*left*) and P^3 (*right*)

on for this example to demonstrate the non-degeneracy in the accuracy of the proposed high order methods when such limiting strategies are applied.

3.2 Examples with Discontinuous Derivatives

In this subsection, we further examine the performance of the proposed methods when applied to examples with discontinuous derivatives. The computation is done with both P^2 and P^3 approximations. That is, $\mathbf{V}_h = \mathbf{V}_h^k$ and the first k time derivatives in (2.1) are used with $k = 2$ and $k = 3$ respectively. In addition, once a mesh element is indicated as a troubled cell, the WENO limiter strategy will be applied in this element. Though the computation is done for both uniform rectangular meshes and unstructured triangular meshes for Examples 3.3–3.7, there is no visible difference in the plots, and therefore only the solutions on triangular meshes are reported in this paper.

Example 3.3 Consider the Burgers equation (3.1) with the same initial and boundary conditions as in Example 3.1. At $t = 1.5/\pi^2$, the solution has developed discontinuous derivatives. The numerical solutions on the unstructured triangular mesh with $h = 1/8$ are shown in Fig. 2. The solution is well resolved for this example. We remark that the proposed method without limiter can also produce non-oscillatory reliable results for this example, and such limiter is more crucial for the cases with some nonconvex Hamiltonians, e.g. Example 3.5.

Example 3.4 Consider the example of (3.2) with the same initial and boundary condition as in Example 3.2. We report the results at $t = 1.5/\pi^2$ when the discontinuous derivative has

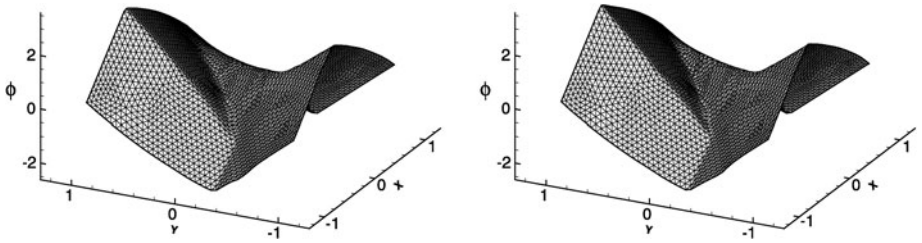

Fig. 4 Two dimensional Riemann problem. The numerical solution at $t = 1$ on the unstructured triangular mesh with $h = 1/20$. P^2 (*left*) and P^3 (*right*)

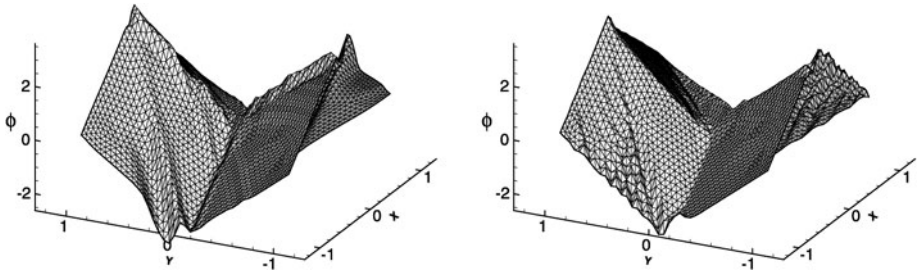

Fig. 5 Two dimensional Riemann problem. The numerical solution without limiter at $t = 1$ on the unstructured triangular mesh with $h = 1/20$. P^2 (*left*) and P^3 (*right*)

developed in the solution. The numerical solutions on the unstructured triangular mesh with $h = 1/8$ are shown in Fig. 3. Both P^2 and P^3 results approximate the viscosity solution very well. And the proposed methods without the limiter procedure also produce non-oscillatory reliable results for this example.

Example 3.5 Consider a two dimensional Riemann problem

$$\begin{cases} \phi_t + \sin(\phi_x + \phi_y) = 0, & -1 < x, y < 1, \\ \phi(x, y, 0) = \pi(|y| - |x|), \end{cases} \tag{3.3}$$

with a nonconvex Hamiltonian and the outflow boundary condition. The results at $t = 1$ on the unstructured triangular mesh with $h = 1/20$ are reported in Fig. 4.

Similar to what was observed in [16, 22], without the limiter procedure, the numerical solutions of the proposed methods do not converge to the viscosity solution for this example, see Fig. 5. In fact, the rarefaction wave is missing and the numerical solution has serious oscillations. On the other hand, the reliable WENO limiter strategies ensure the non-oscillatory results and the convergence of the methods to the correct viscosity solution.

Finally, we want to use this example to compare the computation efficiency of our proposed LW-LSP-DG method and the RKDG method in [16]. In Table 5, the CPU time is reported for these two methods on rectangular meshes. To ensure the linear stability, the *CFL* number for the proposed method is taken to be $2/3$ of that for the RKDG method, see

Table 5 The CPU time (in seconds) of the proposed LW-LSP-DG method and the RKDG method in [16] to compute a two-dimensional Riemann problem

Methods	LW-LSP-DG				RKDG in [16]			
	P^2		P^3		P^2		P^3	
M	0.01	100	0.01	100	0.01	100	0.01	100
40×40	3.42	2.17	21.76	9.81	3.85	2.20	43.15	15.35
80×80	24.18	15.95	158.98	72.68	27.53	16.59	307.92	114.95

Table 6 The percentage of troubled cells subject to WENO limiters for the proposed LW-LSP-DG method and the RKDG method in [16] for a two-dimensional Riemann problem

Methods	LW-LSP-DG				RKDG in [16]			
	P^2		P^3		P^2		P^3	
M	0.01	100	0.01	100	0.01	100	0.01	100
40×40	63.82	5.59	68.91	9.71	63.80	5.84	65.17	7.67
80×80	55.32	4.87	61.67	7.34	55.17	4.94	57.42	5.96

[29]. The time step Δt is determined by

$$\Delta t = CFL \cdot \frac{\min(dx, dy)}{\max_{i=1,2}(\max_{w_1,w_2} |H_i(w_1, w_2)|)}$$

with the maximum taken in the computational domain. In our implementation, the *CFL* number is chosen to be 0.12 and 0.05 for P^2 and P^3 approximations in the LW-LSP-DG methods, and 0.18 and 0.075 for P^2 and P^3 approximations in the RKDG methods. The simulation is performed on a computer with Intel(R) Core(TM)2 Duo CPU P8700 and 3 GB RAM. It is observed that the LW-LSP-DG methods show better computational efficiency than the RKDG methods, especially when the high order polynomial approximation is adopted, even though the *CFL* number for the RKDG methods is 1.5 times of that for LW-LSP-DG methods. This observation is consistent with the facts that the locally curl-free polynomial space has lower dimension and the WENO limiter only needs to be applied once during each time step. In Table 6, we further document the percentages of troubled cells for both methods, which are computed based on the averaging over time. One can see that the larger TVB constant M renders a smaller percentage of troubled cells, and this will reduce the computational cost of the methods when the limiter is involved. In this example, reasonably good numerical results are produced for both $M = 0.01$ and $M = 100$.

Example 3.6 Consider the following example from optimal control,

$$\begin{cases} \phi_t + \sin(y)\phi_x + (\sin x + \operatorname{sign}(\phi_y))\phi_y \\ \quad - \dfrac{1}{2}\sin^2 y - (1 - \cos x) = 0, \quad -\pi < x, y < \pi, \\ \phi(x, y, 0) = 0, \end{cases} \tag{3.4}$$

with the periodic condition, see [27]. And the Hamiltonian is nonsmooth. In Figs. 6 and 7, we report the numerical results approximating the solution ϕ and the optimal control

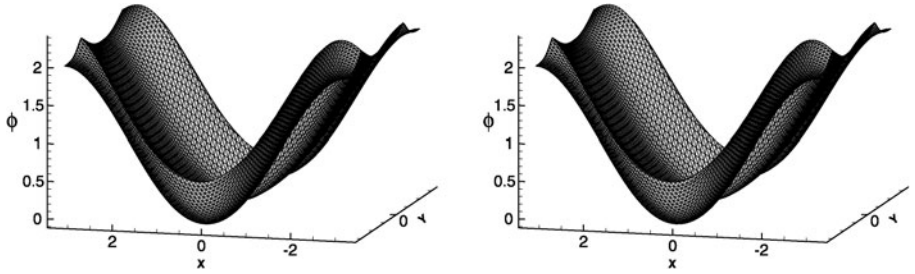

Fig. 6 The optimal control problem. The numerical solution at $t = 1$ on the unstructured triangular mesh with $h = \pi/32$. P^2 (*left*) and P^3 (*right*)

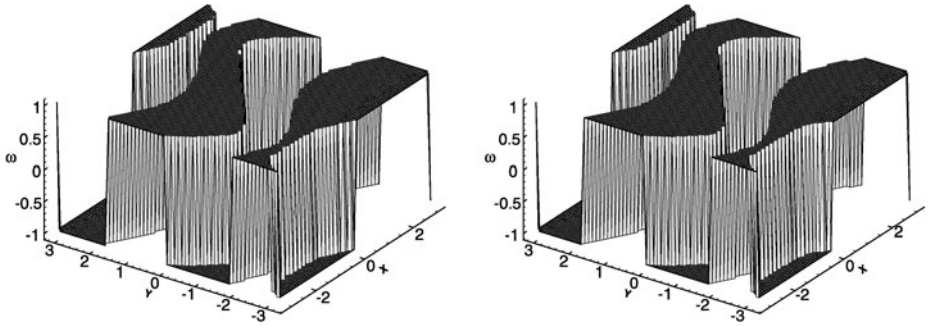

Fig. 7 The optimal control problem. The computed optimal control $\omega = \text{sign}(\phi_y)$ at $t = 1$ on the unstructured triangular mesh with $h = \pi/32$. P^2 (*left*) and P^3 (*right*)

$\omega = \text{sign}(\phi_y)$ on the unstructured triangular mesh with $h = \pi/32$. Note the proposed method computes $\mathbf{w} = \nabla\phi$, and this is very desirable for those problems in which the most interesting information is contained in the first derivative of ϕ, as in this optimal control example.

Example 3.7 Consider the following problem involving a propagating surface [26]

$$\begin{cases} \phi_t - (1 - \varepsilon K)\sqrt{\phi_x^2 + \phi_y^2 + 1} = 0, \quad 0 < x, y < 1, \\ \phi(x, y, 0) = 1 - \dfrac{1}{4}(\cos(2\pi x) - 1)(\cos(2\pi y) - 1), \end{cases} \tag{3.5}$$

where K is the mean curvature defined by

$$K = -\frac{\phi_{xx}(1 + \phi_y^2) - 2\phi_{xy}\phi_x\phi_y + \phi_{yy}(1 + \phi_x^2)}{(1 + \phi_x^2 + \phi_y^2)^{\frac{3}{2}}},$$

and ε is a small constant. The boundary condition is periodic. The local discontinuous Galerkin (LDG) method is adopted to deal with the second derivative terms [10, 16]. This is done in the similar framework as the proposed methods, and the details are not included here for brevity. The numerical solutions for $\varepsilon = 0$ (pure convection) and for $\varepsilon = 0.1$ are plotted in Fig. 8 and Fig. 9 respectively when an unstructured triangular mesh with $h = 1/40$ is used. The surfaces at $t = 0$ for $\varepsilon = 0$ and for $\varepsilon = 0.1$, and at $t = 0.1$ for $\varepsilon = 0.1$, are shifted downward in order to show the detail of the solution at later times.

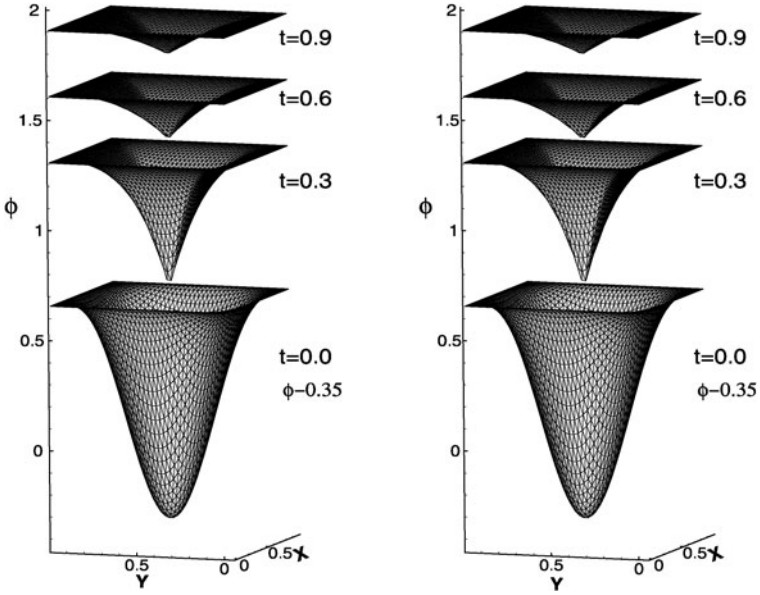

Fig. 8 Propagating surface. The numerical solution on the unstructured triangular mesh with $h = 1/40$, $\varepsilon = 0$. P^2 (*left*) and P^3 (*right*)

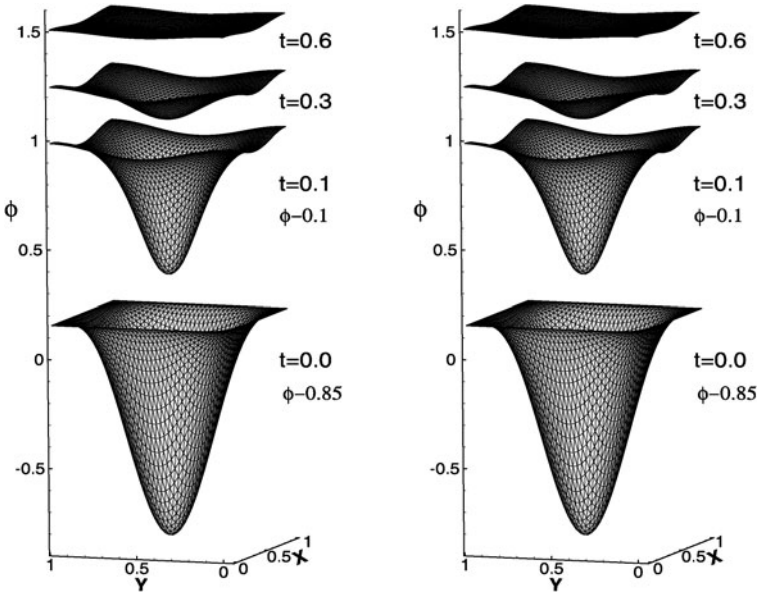

Fig. 9 Propagating surface. The numerical solution on the unstructured triangular mesh with $h = 1/40$, $\varepsilon = 0.1$. P^2 (*left*) and P^3 (*right*)

Example 3.8 We consider the same equation of a propagating surface as in Example 3.7 with the initial condition $\phi_0(x, y) = \sin(\frac{\pi}{x^2+y^2})$, yet defined in a unit disk $\{(x, y) : x^2 + y^2 < 1\}$. A Neumann-type boundary condition $\nabla\phi = 0$ is applied. It is difficult to use rectangular

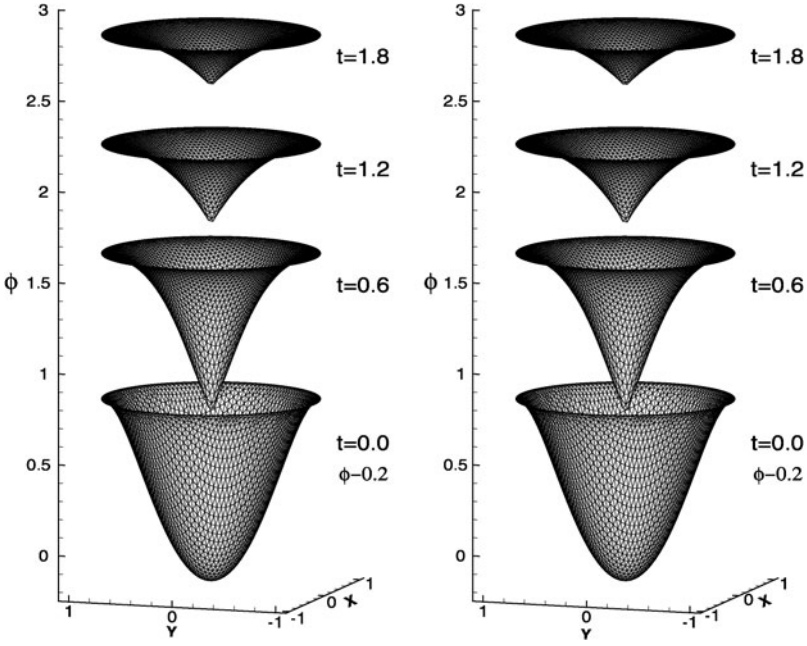

Fig. 10 Propagating surface on a disk. The numerical solution on the unstructured triangular mesh, $\varepsilon = 0$. P^2 (*left*) and P^3 (*right*)

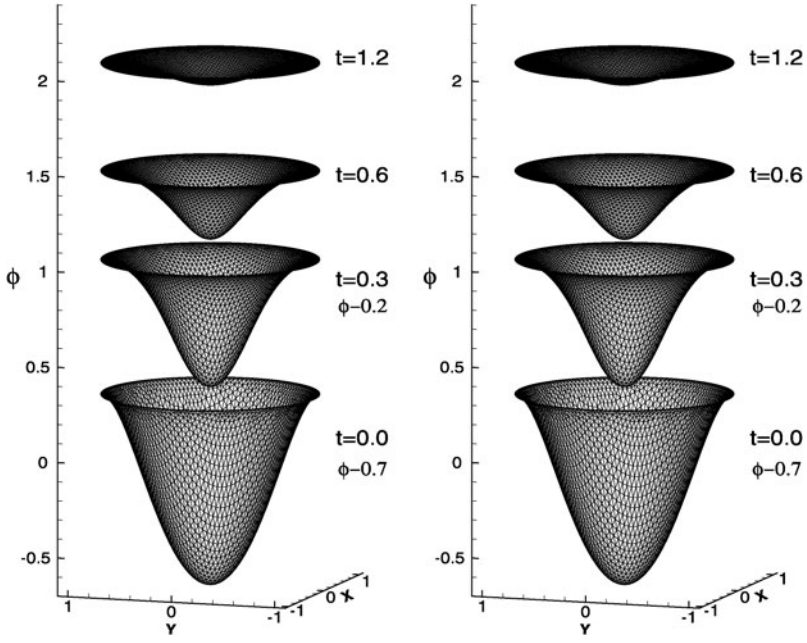

Fig. 11 Propagating surface on a disk. The numerical solution on the unstructured triangular mesh, $\varepsilon = 0.1$. P^2 (*left*) and P^3 (*right*)

meshes for this problem. We adopt an unstructured triangular mesh instead, which consists of 4216 triangles and 2184 nodes. We plot the results of $\varepsilon = 0$ (pure convection) and $\varepsilon = 0.1$ by the proposed method in Figs. 10–11. And the surfaces at $t = 0$ for $\varepsilon = 0$ and for $\varepsilon = 0.1$, and at $t = 0.3$ for $\varepsilon = 0.1$, are shifted downward in order to show the detail of the solution at later times.

4 Concluding Remarks

In this paper, a family of high order numerical methods are designed to solve the Hamilton-Jacobi equation for the viscosity solution. The methods combine the compact one-step one-stage Lax-Wendroff type time discretization, local-structure-preserving discontinuous Galerkin spatial discretization and the robust WENO limiter strategy. Though on unstructured triangular meshes the WENO limiter strategy still relies on relatively complicated reconstruction procedures to achieve high order accuracy, such reconstructions are used only for a small percentage of mesh elements which are identified as troubled cells. Therefore the proposed methods overall involve lower computational complexity and storage usage for both structured and unstructured meshes, while they are capable of capturing the viscosity solutions of Hamilton-Jacobi equations accurately and reliably.

References

1. Arnold, D.N., Brezzi, F., Cockburn, B., Marini, L.D.: Unified analysis of discontinuous Galerkin methods for elliptic problems. SIAM J. Numer. Anal. **39**, 1749–1779 (2001/2002)
2. Bryson, S., Levy, D.: Mapped WENO and weighted power ENO reconstruction in semi-discrete central schemes for Hamilton-Jacobi equations. Appl. Numer. Math. **56**, 1211–1224 (2006)
3. Cheng, Y., Shu, C.-W.: A discontinuous Galerkin finite element method for directly solving the Hamilton-Jacobi equations. J. Comput. Phys. **223**, 398–415 (2007)
4. Cockburn, B., Hou, S., Shu, C.-W.: The Runge-Kutta local projection discontinuous Galerkin finite element method for conservation laws IV: the multidimensional case. Math. Comput. **54**, 545–581 (1990)
5. Cockburn, B., Li, F., Shu, C.-W.: Locally divergence-free discontinuous Galerkin methods for the Maxwell equations. J. Comput. Phys. **194**, 588–610 (2004)
6. Cockburn, B., Lin, S.-Y., Shu, C.-W.: TVB Runge-Kutta local projection discontinuous Galerkin finite element method for conservation laws III: one dimensional systems. J. Comput. Phys. **84**, 90–113 (1989)
7. Cockburn, B., Shu, C.-W.: TVB Runge-Kutta local projection discontinuous Galerkin finite element method for conservation laws II: general framework. Math. Comput. **52**, 411–435 (1989)
8. Cockburn, B., Shu, C.-W.: The Runge-Kutta local projection P1-discontinuous Galerkin finite element method for scalar conservation laws. Math. Modell. Numer. Anal. **25**, 337–361 (1991)
9. Cockburn, B., Shu, C.-W.: The Runge-Kutta discontinuous Galerkin method for conservation laws V: multidimensional systems. J. Comput. Phys. **141**, 199–224 (1998)
10. Cockburn, B., Shu, C.-W.: The local discontinuous Galerkin method for time-dependent convection-diffusion systems. SIAM J. Numer. Anal. **35**, 2440–2463 (1998)
11. Crandall, M.G., Evans, L.C., Lions, P.L.: Some properties of viscosity solutions of Hamilton-Jacobi equations. Trans. Am. Math. Soc. **282**, 487–502 (1984)
12. Crandall, M., Lions, P.L.: Viscosity solutions of Hamilton-Jacobi equations. Trans. Am. Math. Soc. **277**, 1–42 (1983)
13. Dumbser, M.: ADER discontinuous Galerkin schemes for aeroacoustics. In: Proceedings of the Euromech Colloquium, Chamonix, France, vol. 449 (2003)
14. Dumbser, M., Munz, C.-D.: Arbitrary high order discontinuous Galerkin schemes. In: Cordier, S., Goudon, T., Sonnendrcker, E. (eds.) Numerical Methods for Hyperbolic and Kinetic Problems, pp. 295–333. EMS Publishing House, Helsinki (2005)
15. Gittelson, C.J., Hiptmair, R., Perugia, I.: Plane wave discontinuous Galerkin methods: analysis of the h-version. Math. Modell. Numer. Anal. **43**, 297–331 (2009)
16. Hu, C., Shu, C.-W.: A discontinuous Galerkin finite element method for Hamilton-Jacobi equations. SIAM J. Sci. Comput. **21**, 666–690 (1999)

17. Hu, C., Shu, C.-W.: Weighted essentially non-oscillatory schemes on triangular meshes. J. Comput. Phys. **150**, 97–127 (1999)
18. Jiang, G., Peng, D.: Weighted ENO schemes for Hamilton-Jacobi equations. SIAM J. Sci. Comput. **21**, 2126–2143 (2000)
19. Jiang, G., Shu, C.-W.: Efficient implementation of weighted ENO schemes. J. Comput. Phys. **126**, 202–228 (1996)
20. Lax, P.D., Wendroff, B.: Systems of conservation laws. Commun. Pure Appl. Math. **13**, 217–237 (1960)
21. Lafon, F., Osher, S.: High order two dimensional nonoscillatory methods for solving Hamilton-Jacobi scalar equations. J. Comput. Phys. **123**, 235–253 (1996)
22. Li, F., Yakovlev, S.: A central discontinuous Galerkin method for Hamilton-Jacobi equations. J. Sci. Comput. **45**, 404–428 (2010). doi:10.1007/s10915-009-9340-y
23. Li, F., Shu, C.-W.: Reinterpretation and simplified implementation of a discontinuous Galerkin method for Hamilton-Jacobi equations. Appl. Math. Lett. **18**, 1204–1209 (2005)
24. Li, F., Shu, C.-W.: A local-structure-preserving local discontinuous Galerkin method for the Laplace equation. Methods Appl. Anal. **13**, 215–234 (2006)
25. Liu, X., Osher, S., Chan, T.: Weighted essentially non-oscillatory schemes. J. Comput. Phys. **115**, 200–212 (1994)
26. Osher, S., Sethian, J.: Fronts propagating with curvature dependent speed: algorithms based on Hamilton-Jacobi formulations. J. Comput. Phys. **79**, 12–49 (1988)
27. Osher, S., Shu, C.-W.: High-order essentially nonoscillatory schemes for Hamilton-Jacobi equations. SIAM J. Numer. Anal. **28**, 907–922 (1991)
28. Qiu, J.: Hermite WENO schemes with Lax-Wendroff type time discretizations for Hamilton-Jacobi equations. J. Comput. Math. **25**, 131–144 (2007)
29. Qiu, J., Dumbser, M., Shu, C.-W.: The discontinuous Galerkin method with Lax-Wendroff type time discretizations. Comput. Methods Appl. Mech. Eng. **194**, 4528–4543 (2005)
30. Qiu, J., Shu, C.-W.: Runge-Kutta discontinuous Galerkin method using WENO limiters. SIAM J. Sci. Comput. **26**, 907–929 (2005)
31. Qiu, J., Shu, C.-W.: Herimte WENO scheme for Hamilton-Jacobi equations. J. Comput. Phys. **204**, 82–99 (2005)
32. Reed, W.H., Hill, T.R.: Triangular mesh methods for the neutron transport equation. Technical Report LA-UR-73-479, Los Alamos Scientific Laboratory (1973)
33. Shu, C.-W.: TVB uniformly high-order schemes for conservation laws. Math. Comput. **49**, 105–121 (1987)
34. Toro, E.F., Titarev, V.A.: Solution of the generalized Riemann problem for advection-reaction equations. Proc. R. Soc. Lond. **458**, 271–281 (2002)
35. Xu, Y., Shu, C.-W.: Local discontinuous Galerkin methods for high-order time-dependent partial differential equations. Commun. Comput. Phys. **7**, 1–46 (2010)
36. Yuan, L., Shu, C.-W.: Discontinuous Galerkin method based on non-polynomial approximation spaces. J. Comput. Phys. **218**, 295–323 (2006)
37. Zhang, Y.-T., Shu, C.-W.: High-order WENO schemes for Hamilton-Jacobi equations on triangular meshes. SIAM J. Sci. Comput. **24**, 1005–1030 (2003)
38. Zhu, J., Qiu, J., Shu, C.-W., Dumbser, M.: Runge-Kutta discontinuous Galerkin method using WENO limiters II: unstructured meshes. J. Comput. Phys. **227**, 4330–4353 (2008)